THESIS FOR THE DEGREE OF LICENTIATE OF ENGINEERING

Damage and thermally induced defects in railway materials

Casey Jessop

Department of Materials and Manufacturing Technology

CHALMERS UNIVERSITY OF TECHNOLOGY

Göteborg, Sweden 2017

Damage and thermally induced defects in railway materials

Casey Jessop

ISSN 1652-8891

Technical report no 112/2017

Department of Materials and Manufacturing Technology

Chalmers University of Technology

SE-412 96 Gothenburg

Sweden

Telephone +46 (0)31 772 1000

Printed by Chalmers Reproservice

Göteborg, Sweden 2017

To Henry and Josephine ♡

Damage and thermally induced defects in railway materials

Casey Jessop
Department of Materials and Manufacturing Technology
Chalmers University of Technology

Abstract

A major concern for the railway industry today is the problem of rolling contact fatigue (RCF) damage in wheels and rails as a result of increased traffic, accelerations, and loading conditions. The wheel/rail contact condition that occurs in railway applications is complex, and it is essential to understand the associated damage from combined mechanical and thermal loadings in order to predict component life and develop appropriate maintenance systems. The crack initiation and propagation processes of RCF have been extensively studied from both theoretical and experimental points of view; however, certain mechanisms for crack initiation and propagation are still not well understood. Thermally damaged surface layers, often called white etching layers (WELs), seem to contribute to crack initiation. One hypothesis is that such cracks can develop into so-called squats or studs in the rail, and to RCF clusters in wheels. The work presented in this thesis can be separated into two main objectives: the first was to properly describe the three-dimensional (3D) geometry of the network of RCF defects in rails using several characterization techniques, and the second was to study crack initiation from thermally damaged surface spots, which mimic a WEL, using low-cycle fatigue (LCF) tests.

The following methods were used to geometrically describe squat crack networks: high-intensity X-ray radiography complemented with geometrical reconstruction, serial sectioning and metallography in conjunction with microscopy, X-ray tomography, and topography measurements. The experiments were performed on squats from rail sections taken from the field. It was concluded that the different methods are complementary, and observations made using one method can supplement and explain the deficiencies of other methods. Secondly, investigation of crack initiation from thermally damaged surface spots was carried out via strain-controlled LCF experiments using a MTS 809 servo-hydraulic test machine. The effect of initial thermal damage, observed in the form of a small martensite spot (or WEL) on test bars, on fatigue crack initiation was examined and evaluated relative to smooth specimens. Comparisons between the WELs observed in field samples and those produced artificially on test bars and railheads were made regarding microstructure and residual stresses. The presence of initial thermal damage was found to slightly reduce fatigue life.

Preface

This licentiate thesis is based on the work performed in the Department of Materials and Manufacturing Technology between March 2014 and February 2017. The project has been carried out under the supervision of Associate Professor Johan Ahlström and Professor Christer Persson.

The current work is part of activities within the Swedish National Centre of Excellence CHARMEC (Chalmers Railway Mechanics) with additional support from the Vinnova verification for growth programme.

The thesis consists of an introductory section followed by the following appended papers:

Paper 1: 3D characterization of rolling contact fatigue crack networks

C. Jessop, J. Ahlström, L. Hammar, S. Fæster, and H. K. Danielsen, *Wear*, vol. 366–367, pp. 392–400, 2016.

Paper 2: Crack formation in pearlitic rail steel under uniaxial loading: effect of initial thermal damage

C. Jessop, J. Ahlström, and C. Persson

Manuscript

The following paper was not appended to the thesis:

3D characterization of squat crack network using high-resolution X-ray radiography

C. Jessop Ahlström, J., Hammar, L., *The 35th Riso International Symposium on Materials Science: New Frontiers of Nanomaterials*, 2014, pp. 339–348

Table of contents

1. Introduction

1.1. Background

A major concern for the railway industry is the problem of rolling contact fatigue (RCF) in wheels and rails. RCF is a process that arises from the repeated application of loads in rolling contact between materials. This loading causes large stresses within the components, which lead to severe plastic deformation of the topmost layer of the material when the cyclic yield limit in shear is repeatedly exceeded for thousands of cycles [1]. Cracking and increased risk of fracture may occur as a result.

Although railways remain a safer alternative than roads when it comes to the number and severity of accidents that occur every year, some incidents involving trains cause people to lose confidence in the railway system and opt for cars and other means of transportation instead [2]. According to Allianz pro Schiene, based in Germany, the number of deaths per billion passenger–km is orders of magnitudes smaller than those occurring on roads and even buses, at only 0.01 versus 2.77 and 0.16, respectively [3]. It is important to maintain the integrity of railways, and safety is a major concern for the current industry, with several accidents causing widespread recognition of the damage present. For example, in October 2000, a derailment in Hatfield, England that caused four fatalities raised awareness of the importance of maintaining railways for the British railway industry. The Hatfield accident was the result of overlooked severity of RCF in the rails, with inadequate or neglected maintenance being a main cause [4]–[6].

There are many benefits to be gained from researching railway materials. Railway transport has the lowest CO_2 emissions, based on the 2010 International Transport Forum on Greenhouse Gas Emissions, making it an environmentally conscious form of transportation when compared with road and domestic aviation [3]. While road accounted for 72% of transport CO_2 emissions in 2008, and domestic aviation for 5%, rail transport only represented 2%, with 2.7 billion passenger-kilometers and over one million kilometers of lines worldwide [3]. There are many advantages of railways as a means of freight and passenger transport, and the research

undertaken worldwide aims to further improve the environmental, safety, and economic aspects.

Early detection of RCF surface and near-surface defects could help reduce the frequency and intensity of failures and accidents. In order to develop a proper maintenance system, first it is important to understand the nature, cause, and consequences of different types of defects. A better understanding of the mechanisms of crack initiation and propagation, including the influence of climatic conditions and material properties, is necessary to help formulate, calibrate and verify suitable models for crack initiation and propagation.

1.2. Aim

The work within this project can be separated into two main objectives: the first is to properly describe the 3D network of RCF defects in rails using several characterization techniques, and the second is to study crack initiation and propagation through fatigue tests. A good understanding of crack geometry is useful in determining the loading conditions that cause a crack to propagate in a certain manner. Identified loading conditions can later be used for bi-axial testing to obtain RCF crack growth similar to that present in reality. These results can provide relevant information for predicting crack propagation and evaluating the severity of damage during field inspections. At this point, the study of crack initiation and propagation commenced with uniaxial low-cycle fatigue experiments examining the effect of initial thermal damage on fatigue life. Further examination of crack propagation will follow.

2. Theory

2.1. Rolling contact fatigue

Rolling contact fatigue (RCF) is a type of damage that occurs due to repeated application of loads in conjunction with rolling contact between materials. The shear stresses experienced by the rail exceed the yield strength, causing the material in the topmost layer of the railhead to plastically deform, which leads to hardening and realignment of the pearlitic microstructure below the surface. This repeated loading and plastic deformation results in the formation of cracks in the top layer of the rail, as the anisotropy of the microstructure decreases the toughness of the rail in certain directions, creating paths with reduced resistance to crack growth, by which cracks propagate more easily [7]. This fatigue process is becoming more frequent with increased traffic, accelerations, and loading conditions in the railway industry. If not handled correctly, these can pose serious safety and economic risks.

Rolling contact fatigue cracks

Different types of loading conditions in service result in different RCF defect types, some examples of which are shown schematically in Figure 1 [8]. These depend on the location of the contact patch between the wheel and the rail as well as the contact condition, both of which vary with wear and with profile changes of the components.

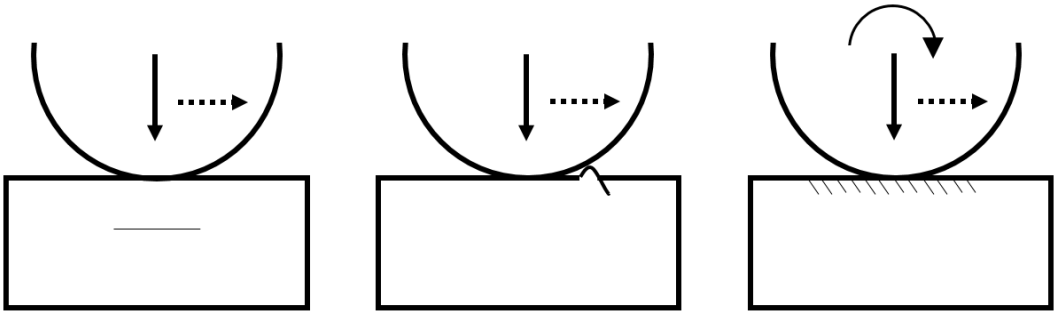

Figure 1. Different types of contact loading and the resulting crack formation. Modified from [8].

In the last few decades, awareness of so-called “squats” has increased due to higher occurrence of this type of service-induced defect. Some examples of squats are shown in Figure 2. The name originated from the apparent shape of the crack formation on the surface of the rail, which looks as though a heavy gnome squatted on the rail, leaving an indentation of two lobes of similar size. The two-lobe form on the surface of a rail suggests a planar crack network below the surface, causing internal wear within the crack. This in turn causes the rail surface to sink and take on a darker appearance due to less surface wear. Metallographic cross-sectioning shows an initial crack growing at small angles, around 10° to 30°, from the surface of the rail and then deviating to propagate nearly parallel to the surface within a shallow depth [9]. In the early stages of growth, squats resemble commonly occurring cracks often referred to as ‘head checks’. Head checks, such as those shown in Figure 3, occur on the gauge corner of high rails in shallow curves [10]. Generally this type of RCF defect is not a cause for major concern, since a combination of wear, regular maintenance and grinding removes the thin layer in which the cracks are present. In some cases, such as those shown schematically in Figure 4, the cracks can branch upwards towards the surface as it progresses [11], causing spalling (far-right image in Figure 2 and Figure 4b), which leads to increased impact loading on further traffic. The crack growth can also deviate into a downwards angle, leading to increased risk of rail break (Figure 4c) [12].

Squats are surface- or near-surface-initiated defects, thought to originate due to local plastic deformation of the surface as a result of RCF loading, including dynamic wheel/rail contact forces [12], [13]. Some types of squats, in which local thermal damage to the rail surface affects the initiation mechanism, are often referred to as studs [13], [14]. However, it should be noted that the distinction between squats and studs is not always made [12], [15]–[20]. A stud (squat-type defect) is not formed due to severe plastic deformation of the surface pearlite layer, but develops in un-deformed pearlite and propagates through grains [14].

Figure 2. Examples of squats of different severity in field, as well as an example of spalling (far right).

Figure 3. Commonly occurring RCF defects on the gauge corner of rails. Dashed lines highlight the curvature of the head checks from the gauge corner into the running band.

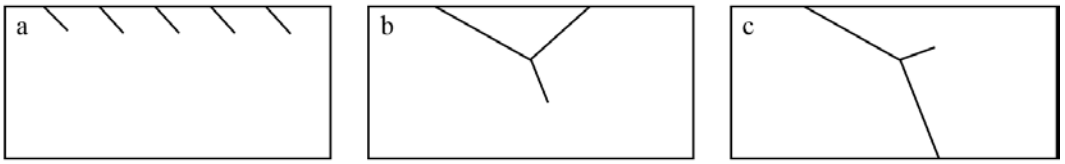

Figure 4. Schematic showing three levels of severity of RCF cracks on rail surface: (a) small cracks, (b) spalling, and (c) risk for rail break. (Longitudinal section)

Thermal damage initiation mechanisms

Thermal loading, or damage, can have an effect on RCF crack formation. For example, white etching layers (WEL) can form during excessive braking or acceleration. When the temperature at the point of wheel/rail contact exceeds the effective austenitization temperature (roughly 800 °C [21]) and is then rapidly cooled, a thin layer of martensite can form on the surface. Due to this thin layer's higher resistance to Nital etching, it appears white (unetched) under optical microscopy (Figure 5a) [22], [23]. For this reason, it is commonly called a white etching layer (WEL). WELs are much harder and have more brittle behavior than

the bulk material, which increases the risk of cracks initiating at the site. Crack initiation related to WELs is a common problem in the railway industry that is observed in both rails and wheels. There are generally two types of associated cracks: those that grow at the interface of the WEL and the bulk material (Figure 5b), and those that grow through the WEL (Figure 5c). Figure 5b shows the tendency of cracks to branch at the interface and propagate perpendicular to the original crack, along the bottom of the WEL.

Additionally, residual stresses arise in rails due to the formation of WELs. They are caused by the changes in volume caused by thermal expansion on local heating, leading to plastic deformation, and volume expansion on phase transformation from pearlite via austenite to martensite. This further increases the risk of crack initiation at these thermally affected areas [24].

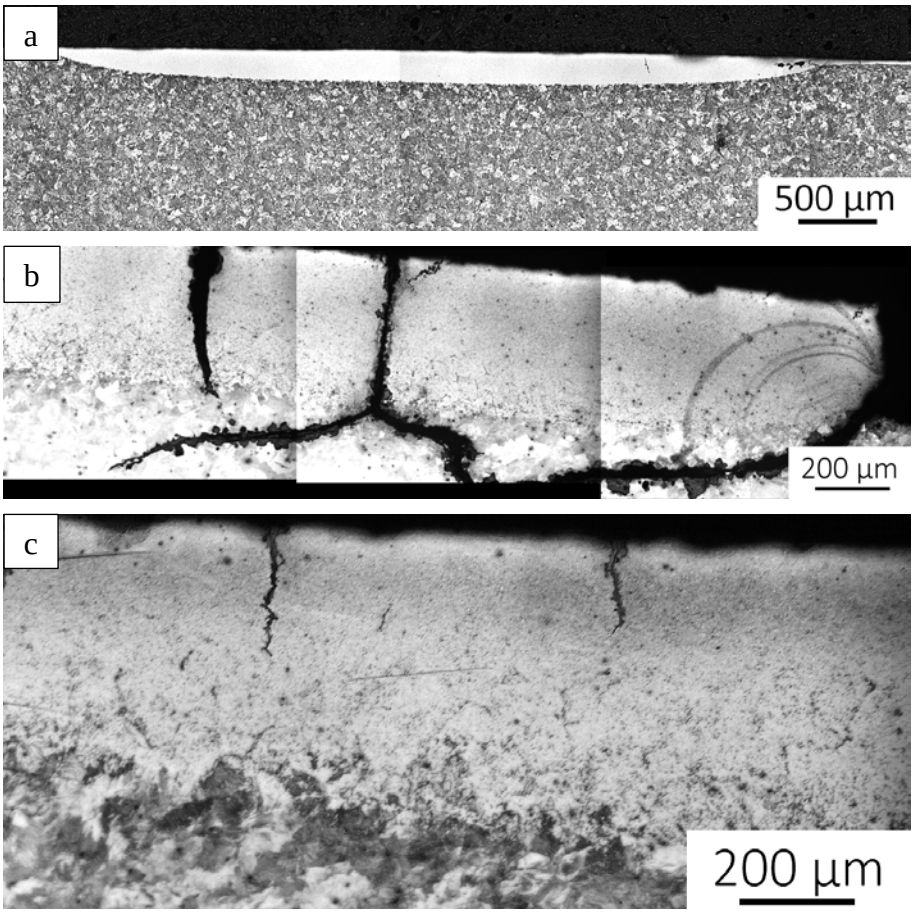

Figure 5. Examples of WELs taken from the field: (a) overview of WEL on rail surface, (b) close-up of cracks growing at interface of WEL and bulk surface, and (c) through WEL.

2.2. Residual stresses

During operation, the application of loads in conjunction with rolling of the wheels on the rails introduce stresses of magnitudes enough to plasticize the material; the stresses that remain in the material after the load is removed are referred to as residual stresses. These stresses are observed as deformations within the crystal lattice. The presence of residual stresses can have positive or negative effects on fatigue life and crack growth rates, depending on their magnitude and whether they are compressive or tensile. While compressive residual stresses tend to hinder crack growth, tensile stresses can increase rates of crack propagation [25].

X-ray diffraction (XRD) is an analysis method that provides information on the atomic and molecular structures of crystalline materials. This technique makes it possible to identify the diffraction peaks of crystalline phases of an investigated sample. It can therefore be used for residual stress measurements by comparing the measured peaks to those of a stress-free specimen.

The principle of the technique is based on X-ray diffraction linked with elastic scattering of electrons, and the high-energy electromagnetic radiation of X-rays. The diffraction mechanism consists of an incoming X-ray wave, initially confined to a single direction, which interacts with the crystals in a sample and diffracts in different directions depending on the symmetry of the unit cell. This interference is shown schematically in Figure 6, and follows Bragg's law:

$$n\lambda = 2dsin\theta$$

Where n is an integer value, λ is the wavelength of the incident wave, d is the inter-planar spacing, and θ is the angle between the incident X-ray and the atomic plane [26]. In steels, the penetration depth of X-rays is limited to approximately 5 μm below the surface.

A peak shift in the diffraction pattern indicates a strain in the material caused by an increase or decrease (elongations or contractions) of the inter-planar spacing in the crystal lattice. The measurement of residual stresses is calculated assuming a plane stress state; that is, the stress normal to the surface is zero [27].

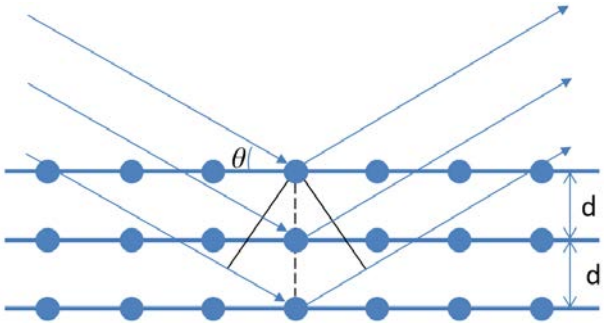

Figure 6. X-ray diffraction; *d* is the spacing between the atomic planes, and θ is the angle between the incident X-ray and the atomic plane.

The strains can be calculated in terms of inter-planar spacing using the aforementioned set-up, but it is more useful to know the residual stresses in the sample. The $\sin^2\psi$ method is the technique most commonly used for residual stress analysis. The measurements taken at chosen $\sin^2\psi$ angles are plotted against the inter-planar spacing, and the stress can be determined from the following relation [27]:

$$\sigma_\varphi = \frac{E}{1+\nu} m$$

Where E is Young's modulus, ν is Poisson's ratio, and m is the gradient of the d versus $\sin^2\psi$ curve.

2.3. Fatigue

Low-cycle fatigue

The low-cycle fatigue (LCF) life of a material is characterized by the strain-life (Coffin-Manson) curve, a log-log plot of the plastic strain amplitude versus number of cycles to failure, according to the following equation [28]:

$$\varepsilon_{\mathrm{pa}} = \varepsilon_{\mathrm{f}}'(2N_{\mathrm{f}})^c$$

Where $\varepsilon_{\mathrm{ea}}$ is the plastic strain amplitude, ε_{f}' is the fatigue ductility coefficient, N_{f} is the number of cycles to failure ($2N_{\mathrm{f}}$ is the number of reversals to failure), and c is the fatigue ductility exponent. ε_{f}' and c are considered material properties [29].

For strain-controlled fatigue tests, which are commonly used for LCF, the specimen is cycled between a maximum and minimum strain, and the stress response is measured. The relationship between the stress and strain at each cycle is presented in the form of a hysteresis loop (an example is shown in Figure 7). The Bauschinger effect is evident in the first cycle, i.e. after the first tension loading, the material yields at lower stress upon reversed loading. There is typically an initial transient in the stress amplitude, but after some cycles the behavior stabilizes and the stress amplitude varies less until larger cracks develop, resulting in a decreased peak stress level. Eventually, cracks grow to cause failure of the specimen.

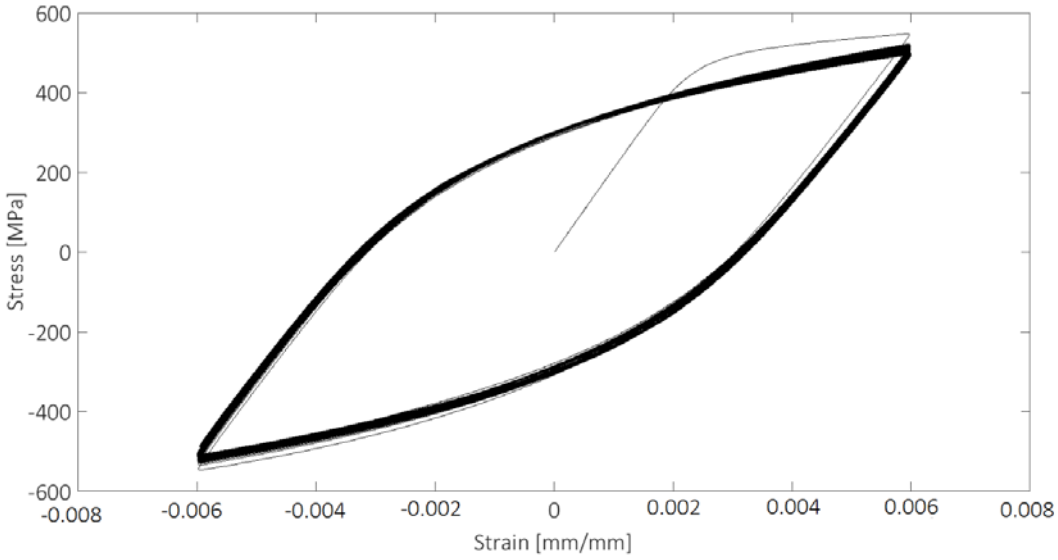

Figure 7. Typical hysteresis loops for strain-controlled LCF test in uniaxial cyclic loading, with constant total strain amplitude of 0.6% in this case. The stress amplitude registered in this case decreases throughout the test.

High-cycle fatigue

High-cycle fatigue (HCF) occurs when a material is subjected to relatively low loads (compared to the yield stress) in order to have deformations in the elastic range. Generally this is defined as lifetimes exceeding some 10^4 cycles, in which case a stress-based approach is preferred for fatigue testing. The fatigue life is generally represented in a stress-life (S-N) curve. The fatigue life is dependent on the stress amplitude according to the following:

$$\sigma_{\mathrm{a}} = \sigma_{\mathrm{f}}'(2N_{\mathrm{f}})^{b}$$

Where σ_a is the stress amplitude, σ_f' is the fatigue strength coefficient, N_f is the number of loading cycles to failure, and b is the fatigue strength exponent [29]. The number of cycles that a material can endure until failure decreases as the maximum stress amplitude increases [28]. The mean stress effect is important in the study of HCF, and it can be described using the modified Goodman relationship:

$$\frac{\sigma_a}{\sigma_{ar}} + \frac{\sigma_m}{\sigma_f'} = 1$$

Where σ_{ar} is the equivalent stress amplitude, and σ_m is the mean stress. That is, σ_{ar} is the stress amplitude that gives the same fatigue life with zero mean stress as that from a particular case with the given stress amplitude of σ_a and mean stress of σ_m. Using this equivalent stress amplitude, the fatigue life can be evaluated using a more general form of the stress-life equation [29]:

$$\sigma_a = (\sigma_f' - \sigma_m)(2N_f)^b$$

3. Materials

The materials investigated in this work were: rail steels taken from the field (from different operators and providers within Europe) for the damage characterization studies, as well as R260 rail steel (typical composition is shown in Table 1) for the experiments on virgin material using the axial-torsional testing machine. Figure 8 shows a description of the transverse and longitudinal sections of a rail section taken from the field.

Table 1: Typical composition of R260 steel. In wt%.

C	Mn	Si	P	S	Cr	Al	Fe
0.74	1.08	0.30	0.013	0.018	0.040	0.003	Balance

Fatigue experiments were performed on specimens with geometry as shown in Figure 9. Tests were performed at room temperature on both smooth test bars and test bars with initial thermal damage. The un-notched specimens were used to provide a basis for the fatigue behavior of the material. The initial thermal damage was made with laser heating experiments.

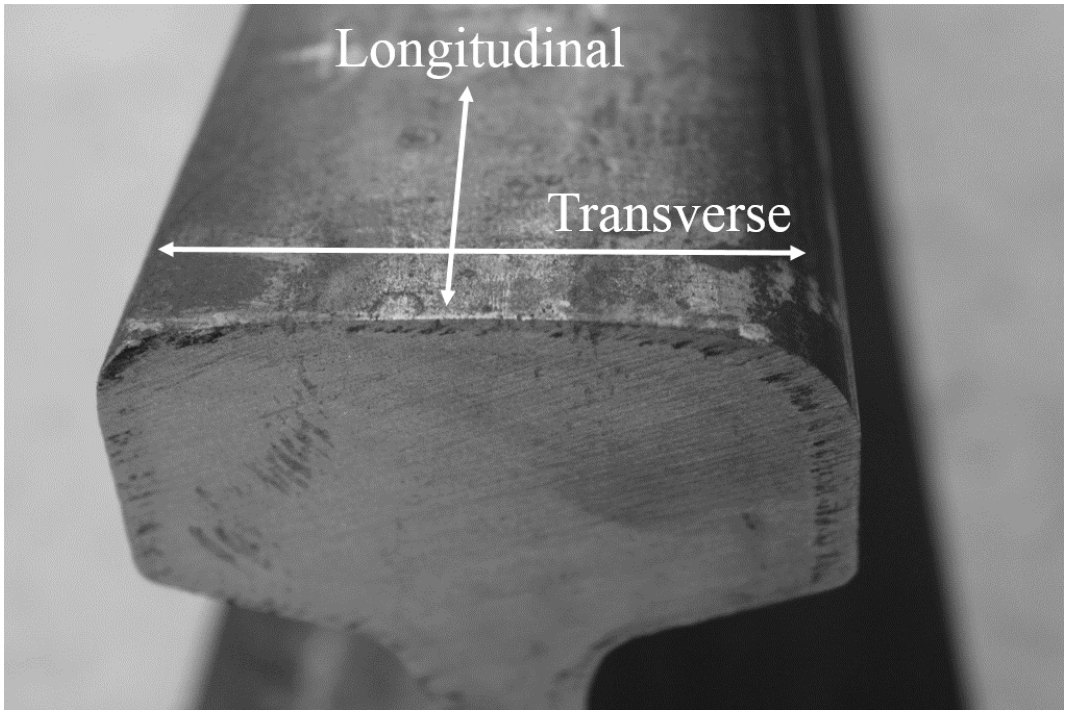

Figure 8. Rail section from the field. The width of the rail is approximately 70 mm.

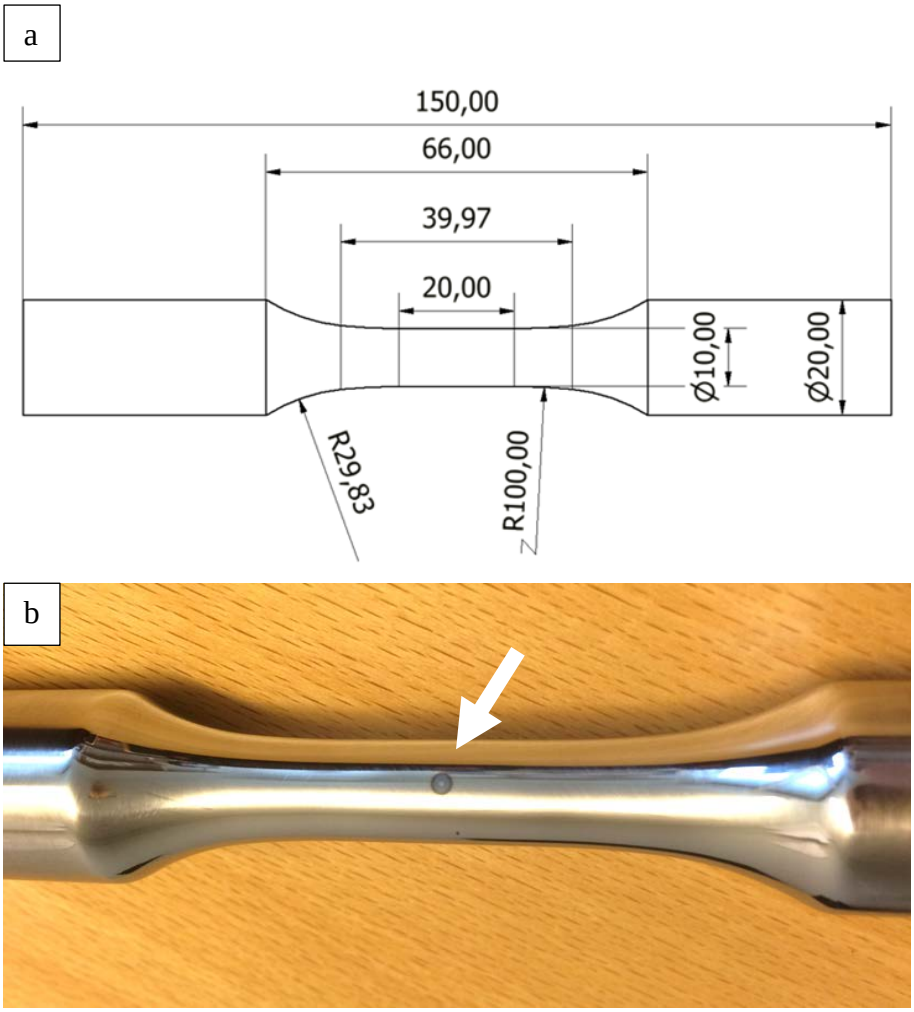

Figure 9. a) Specimen geometry, b) arrow points to WEL on test bar.

4. Experimental methods

4.1. Characterization of RCF damage and defects

Microscopy

Microstructural evaluation is carried out to understand the observed relations between material microstructure and mechanical properties. Sample preparations were made, including surface finishing (grinding and polishing) and etching, according to the specimen and to the purpose of the investigation. All grinding and polishing was done using Struers preparation equipment, and etching with Nital 3% for different amounts of time. Investigations were carried out using optical microscopy, stereomicroscopy, and scanning electron microscopy (SEM). Optical microscopy allows for an overview of the microstructure, including pearlite orientation and deformation. Stereomicroscopy allows for inspection of rough surfaces and lower magnification. However, the depth of focus is not sufficient to obtain clear images of a textured surface, which requires the use of SEM. This technique allows for better spatial resolution, depth of focus, and higher magnification. The instruments used in this work were: a Leitz DMRX optical microscope, a Zeiss SteREO Discovery V20 stereomicroscope, and a LEO 1450VP SEM.

X-ray imaging technique

Radiographic investigation was carried out on a rail sample from the field, in which four squats were present. The squat shown in Figure 10 was radiographed and subjected to metallographic preparation. Two pairs of crossed golden wires (GC1 and GC2 in Figure 10) were fixed on the surface of the rail in order to locate the squat network in two dimensions (x and y) in each image. A geometrical analysis was carried out on the images in order to obtain the third dimension (z) required for the 3D reconstruction of the crack network (Figure 11). The midpoint between the gold crosses corresponds to y=0 mm, while the horizontal line in Figure 10 defines the position x=0 mm. The radiography technique is fully described in Paper 1.

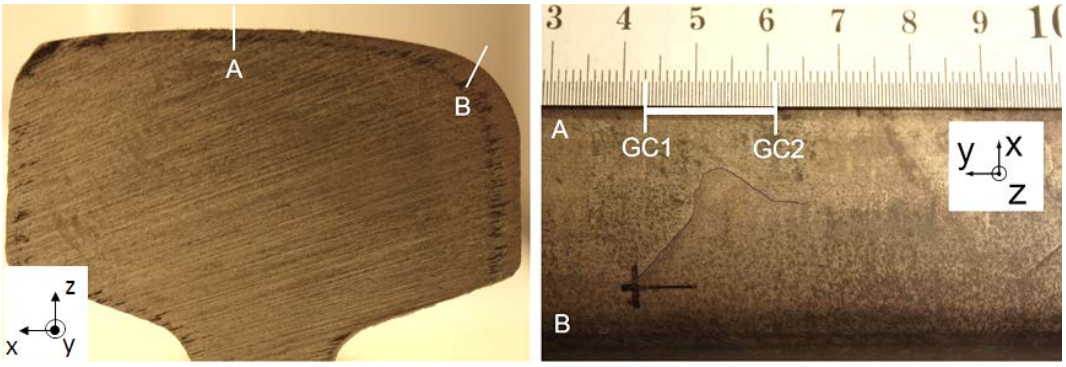

Figure 10. Squat with gold cross marks (GC1, GC2) and scale
(the V-shaped surface-breaking crack has been traced to make it more visible).

Geometrical reconstruction

In the field, rails are only accessible from the top and sides, rendering conventional tomography impossible and necessitating a modified geometrical reconstruction. A combination of visual inspection, a mathematical model, and semi-automated data processing was developed based on certain characteristics of the radiographs. When parts of the crack are parallel to the X-ray beams, good contrast is obtained in the radiograph. The crack plane is thus calculated from the positions in which the line profile provides high contrast in the different projections.

The part of the crack that provides the highest contrast is selected, shown as P_1 and P_2 in Figure 11a. The distance between the points, P_1P_2, is assumed to be a straight line where the radiation is piecewise parallel to the crack. A plane, S_n, is obtained from the vector $\overrightarrow{P_1P_{2_n}}$ and the point P_0 (Figure 11b). When the object has been rotated by an angle $\Delta\theta$ (Figure 11c), new points P_1 and P_2 are selected. A new vector $\overrightarrow{P_1P_{2_n}}$ is obtained, and the next plane, S_{n+1}, is calculated. The lines of intersection between the individual planes and the vectors $\overrightarrow{P_0P_1}$ and $\overrightarrow{P_0P_1}$ give the endpoints of each plane. The midpoint between intersection line endpoints is equal to the tangent to the crack plane, which gives the z-coordinate of the crack. The result was plotted in Matlab [20].

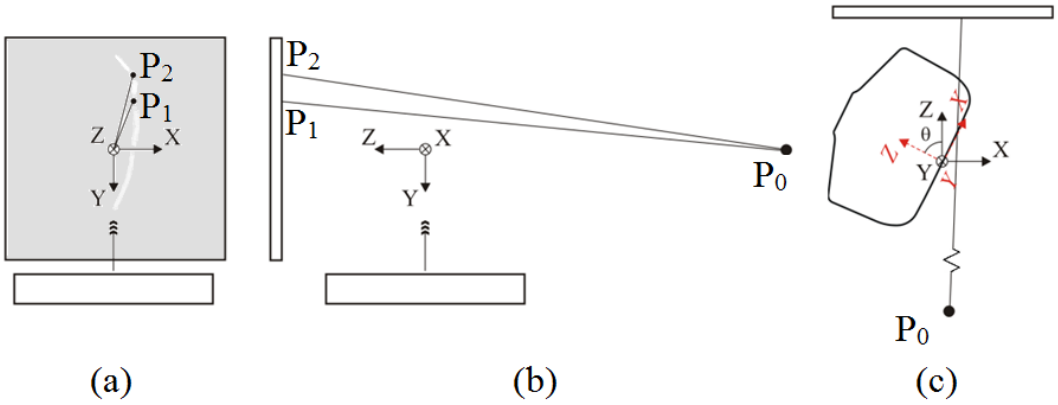

Figure 11. Radiographic set-up and system for geometrical reconstruction: (a) front view and (b) view from left, both showing rotation table and symbolic detector, and (c) top view, showing rail sample and symbolic detector.

Metallography

Metallographic cross-sectioning was done on the rail sample in Figure 10. The series of sections obtained were analyzed using image processing in Matlab to position the depth of the crack relative to the surface. The curves from metallography were compared to the 3D reconstruction at given coordinates in order to determine the accuracy of the geometric reconstruction method.

X-ray tomography

A piece of a different rail was examined using a Zeiss Xradia 520, in collaboration with researchers at the Technical University of Denmark (DTU). X-ray tomography is a technique which takes a series of 2D images through a rotating sample. The contrast in the images relates to the relative absorption of X-rays (proportional to density), and the tomography method combines them in order to numerically build a 3D representation of the sample [30], [31]. The use of this method provides information about the internal crack networks, including branching and topographic information.

Surface topography

A Somicronic Surfascan 3D stylus-based surface profiler was used to obtain 3D mapping of regions of interest on the bulk-side crack surface of a squat taken from the field, shown in Figure 12. The rail surface was cut strategically in order to

remove as much excess steel as possible without damaging the crack network. Cuts were made on either side of the surface-breaking crack so that they just reached the crack network from the side. The railhead was immersed in liquid nitrogen to embrittle the steel, after which the top of the squat network was removed by impact loading.

The profiler was fitted with a ST027 stylus probe (2 mm tip radius and a 90° tip angle), and an accurate depth description was acquired. An overall geometry was obtained using a 1-mm step size over the 40 x 40 mm^2 area of the squat, while detail maps were done on smaller regions with a step size of 50 µm to allow for the ridges seen on the surface to be measured. The procedure for removing the surface of the rail removed some edges of the crack network (see left side of Figure 12b). However, beach marks are apparent in the direction perpendicular to the running direction, confirming the fatigue nature of the squat growth.

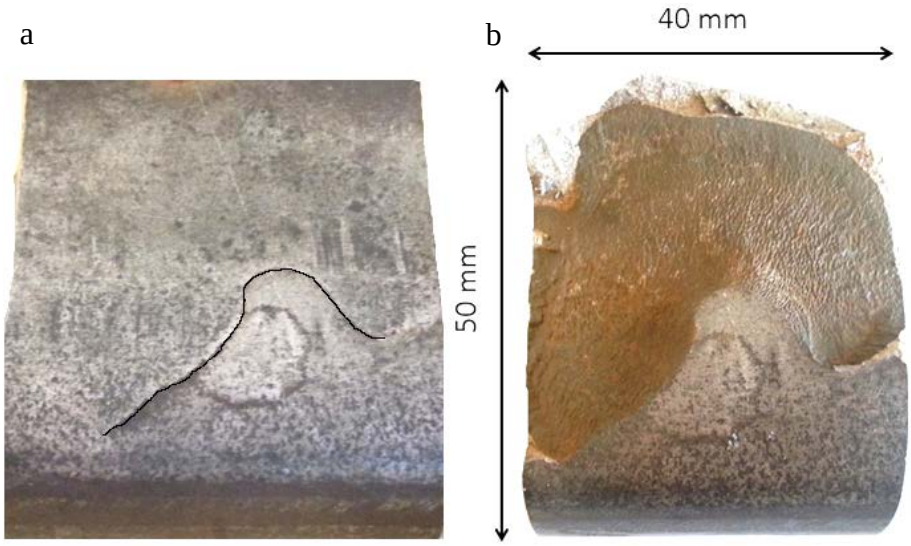

Figure 12. Surface of rail with squat before (a) and after (b) being opened for topography measurements.

4.2. Residual stress measurements

Residual stress measurements were done using a Stresstech Xstress 3000 X-ray machine with the $\sin^2\psi$ method and Cr Kα-radiation, with 1 mm and 3 mm

collimators used for measurements on test bars and rail sections, respectively. The set-up is shown in Figure 13, with two detectors (A and B in Figure 13a) positioned in order to include the ferrite peak at $2\theta \approx 156°$, allowing for simultaneous collection of two 2θ angles [27]. The measurements were run with the inclination angle ψ between -45° and +45°, using nine equal steps in $\sin^2\psi$ (i.e. 0°, ±21°, ±30°, ±38°, ±45°), and in 3 directions (Φ=0°, 45°, and 90°).

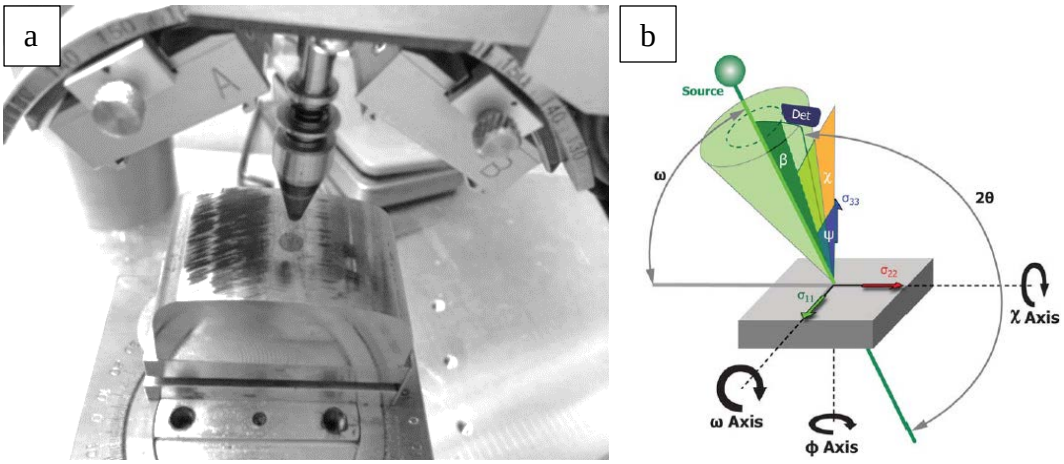

Figure 13. (a) Stresstech Xstress 3000 X-ray machine setup, and (b) chi mode diagram for residual stress measurements [32].

Residual stress measurements were taken on and around martensite spots formed on rail samples with laser heating experiments carried out at Trumpf GmbH, Ditzingen, Germany. A TruDiode laser was used in order to form secondary martensite spots in the WEL band of a rail section taken from the field. The same parameters were used to make martensite spots in the center of the running band of the new rail section. The spots were 6 mm in diameter, and the purpose was to determine the state of residual stresses resulting from thermal damage. In addition, 2-mm spots were formed on test bars in order for use in fatigue tests (the results are presented in Paper 2). The pulse shapes for the two sizes are shown in Figure 14b, and the diameters stated above refer to the diameter of the laser beam on the steel surface. The WEL spots were examined using stereomicroscopy (Figure 26), and residual stress measurements were taken on the surface of the 6-mm spots on both

used and new rail sections. The presence of martensite was confirmed via Nital etching and micro-hardness measurements.

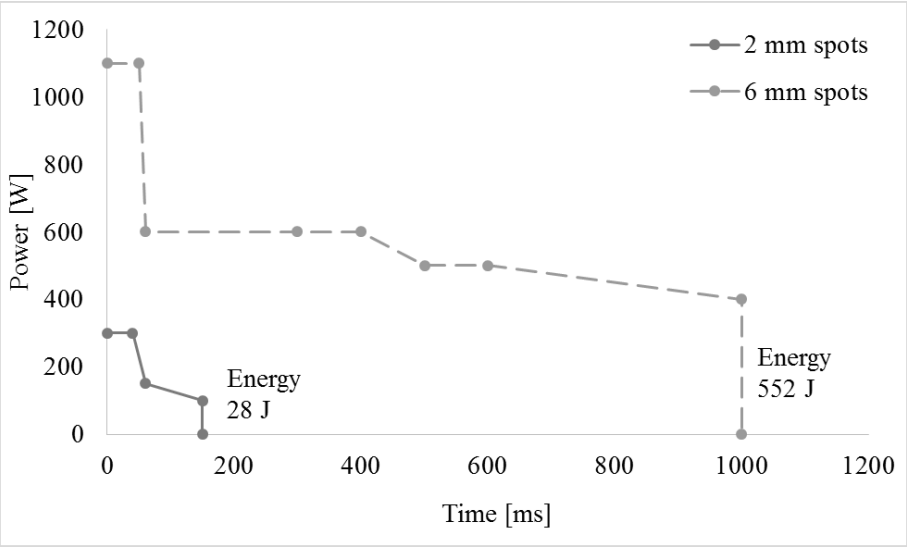

Figure 14. Laser energy pulse shapes for formation of 2 mm spots (solid line) and 6 mm spots (dashed line).

4.3. Fatigue testing

Mechanical testing is used to determine the stress-strain behavior of a material during mechanical loading, which can be either uniaxial or multiaxial. Experiments can be run either in stress- or strain-control. An MTS 809 axial/torsional testing system, the testing area of which is shown in Figure 15, was used for fatigue testing in this project. Uniaxial strain-controlled fatigue tests were performed at room temperature, at a total strain rate of 10^{-2} s^{-1} and at three different constant strain amplitudes: 0.4%, 0.6%, and 1.0%. Test bars were machined, ground and polished before testing. Two different conditions were tested: un-notched and with initial thermal damage, Figure 9. The un-notched specimens were tested to provide a basis for the low-cycle fatigue behavior of the material. The thermal damage was in the form of a WEL spot with thickness close to 200 μm, a thickness commonly found in field, formed by laser-heating a spot on the polished test bar.

Figure 15. Experimental set-up for LCF damage initiation tests.

5. Summary of results and discussion

5.1. Characterization of RCF damage and defects

The RCF damage in the rail sections taken from the field was examined using serial sectioning techniques with optical microscopy (OM), and scanning electron microscopy (SEM). The crack network geometry was also examined using stereomicroscopy, high-intensity X-ray radiography complemented with geometrical reconstruction, X-ray tomography, and topographic measurement techniques.

Plastic deformation

Metallographic investigation of rail sections taken from the field allowed for a closer look at the area within and around the crack, providing better insight into the mechanisms involved in crack propagation, such as plastic deformation and possible thermal damage. It was found that plastic deformation had occurred, mostly around the surfaces of the crack. However, it is not seen along the entire length in the transverse sections. This could be an effect of mixed mode loading of the crack, not excluding the possibility that other mechanisms are contributing to crack growth, such as water entrapment, wedge effects, etc. In some sections examined, the deformation of the pearlite microstructure can be seen in the OM image in Figure 16. Around the crack opening, the deformation of pearlite grains was clearly seen, shown in Figure 17. Realignment of grains was apparent at certain areas along the crack (see Figure 18a); however, some areas seem unaffected, as shown in the different SEM micrographs in Figure 18. This suggests the crack did not grow following the severely deformed microstructure, and that other parameters affect the growth path through the bulk of the material.

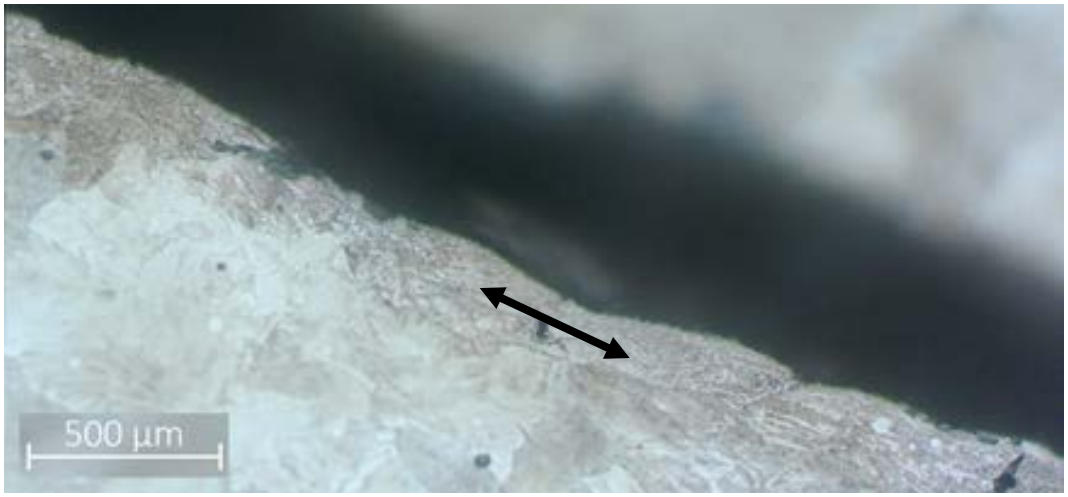

Figure 16. OM image of pearlite colonies deformed along the crack face.

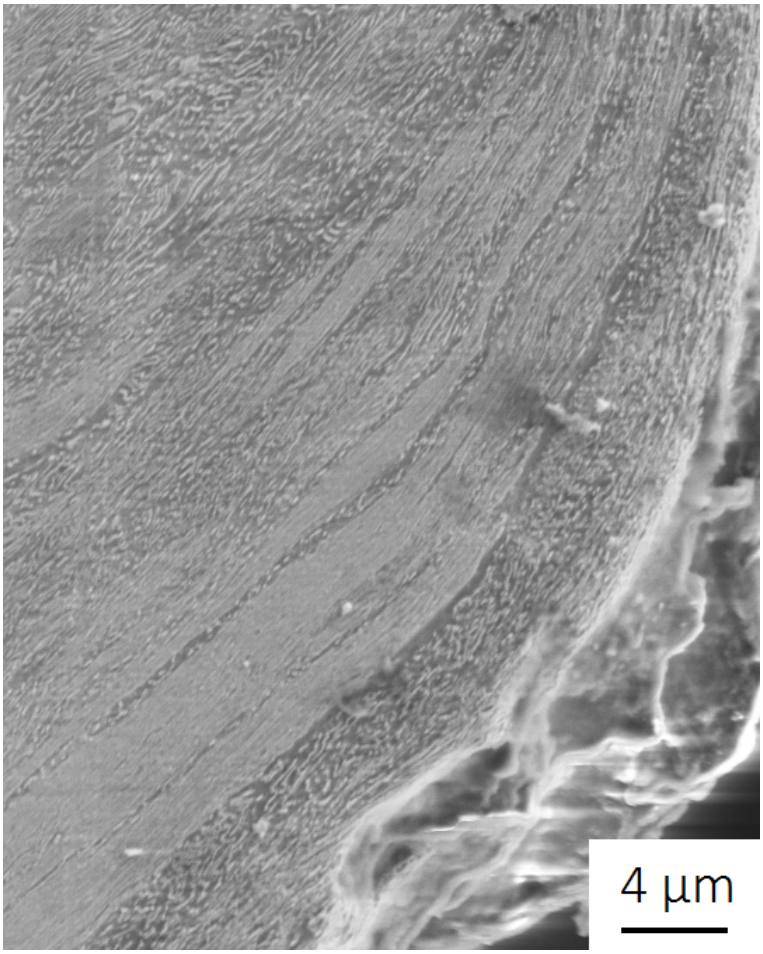

Figure 17. Deformation of pearlite colonies along the edge of the crack opening.

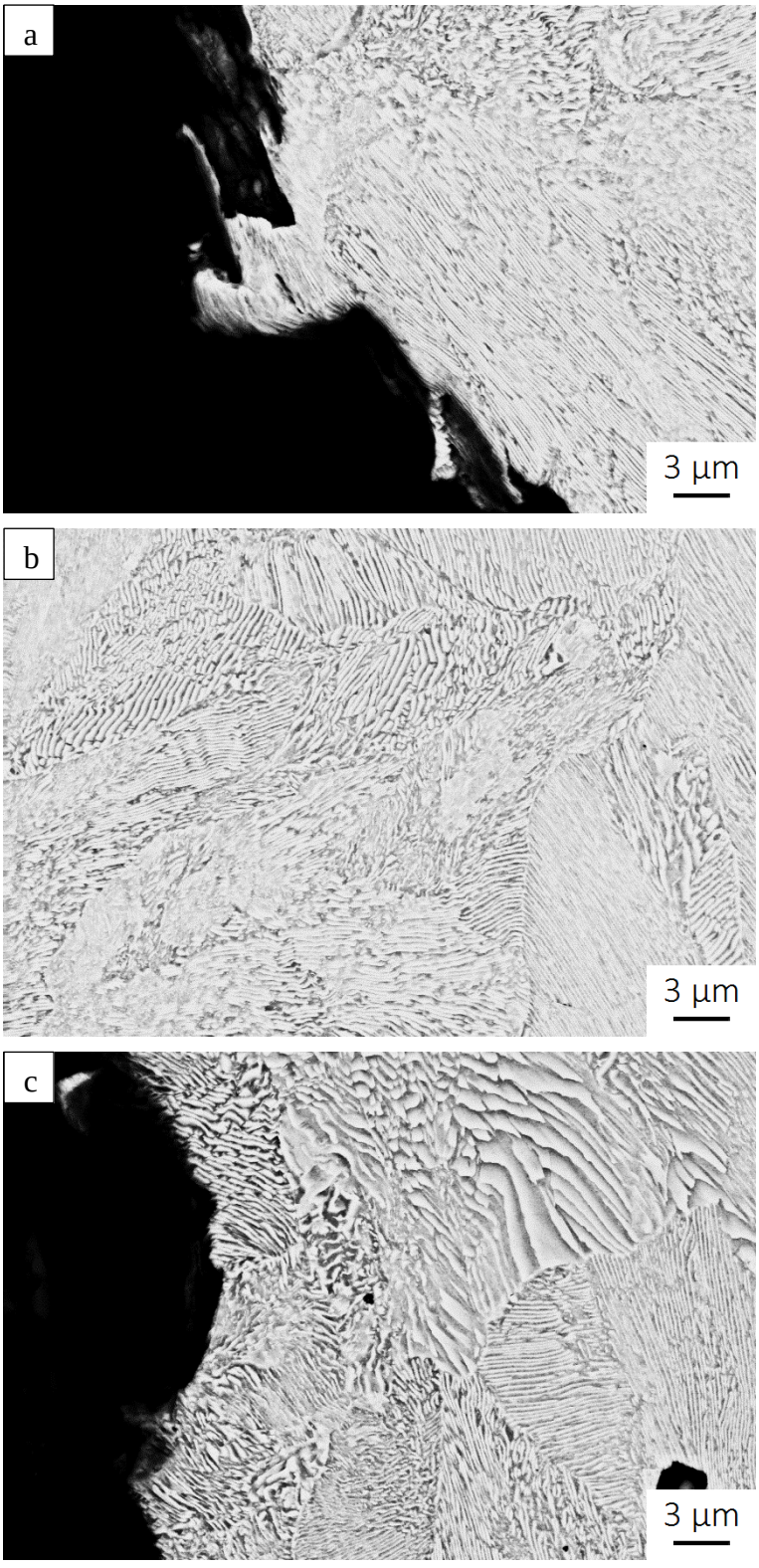

Figure 18. Backscattered electron (BSE) SEM micrographs showing plastic deformation and realignment of pearlite along the crack in (a), compared to the bulk material (b). Randomly oriented pearlite grains can be seen in (c).

Thermal damage

Thermal damage is often found on railheads, and initial inspection of a rail section taken from the field showed quite severe spalling occurring on the surface, in addition to a large thermally damaged strip, the origination of which cannot be determined (Figure 19). The surface was cleaned and etched using Nital in order to reveal the presence of a white etching layer (WEL). The WEL suggests there was some thermal damage that transformed a thin layer of the pearlitic/ferritic material into martensite. Many small cracks are seen within this layer, which highlights the brittle nature of the martensite.

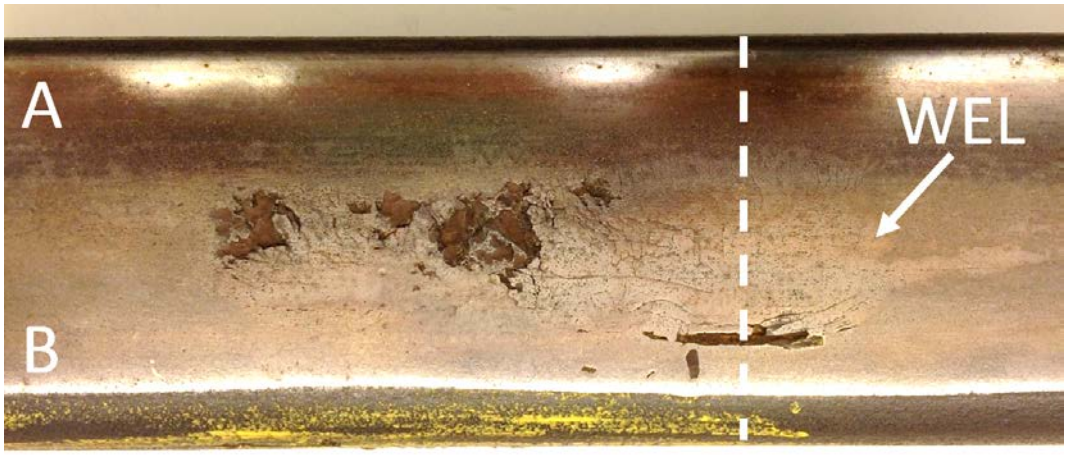

Figure 19. Rail surface after Nital etching: spalling off of large sections is observed in the running band. Section location is shown with a dashed line.

Upon sectioning as shown in Figure 19, the depth of the damage can be more closely examined, including crack patterns and crack depths in the different parts. Sections were prepared for inspection using optical and stereomicroscopy. Thermal damage can be observed in Figure 20. Some cracks in the cross-section reach more than 1 mm in depth, while smaller cracks (150 and 200 μm) are found close to the field side. A closer look at the WEL (Figure 20b) shows that there are in fact two different WELs present: a thin (~200-μm) layer appears above a thicker (~550-μm) layer on the surface. The presence of two layers should be the result of multiple occurrences of thermal damage (e.g. wheel burns) on the same place. The primary layer exhibits a heat-affected zone, appearing darker just below the secondary layer,

which suggests some tempering of the martensite accompanying a second heating event [33]. Furthermore, near the bottom-right corner of Figure 20a deep cracks are present, traveling through the WEL and along the transition between the WEL and bulk material. This could be due to the rolling contact loading occurring between the wheel and rail, affecting the harder and more brittle material within the WEL as well as causing localized strain concentrations beneath the harder layer. The same crack is shown in Figure 5.

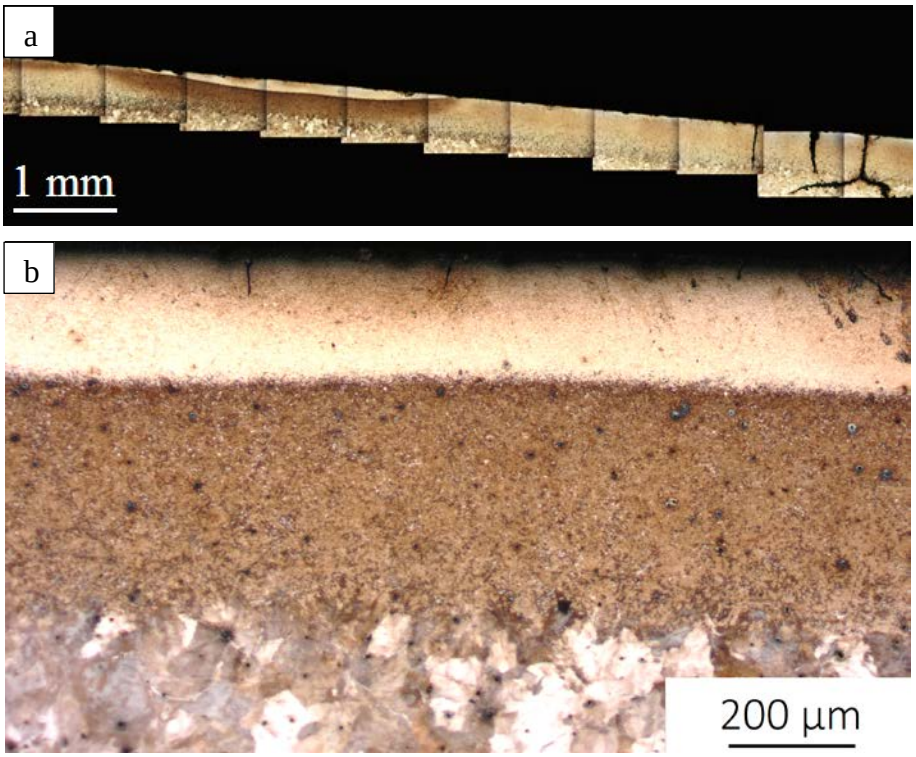

Figure 20. (a) WEL on cross-section from optical microscopy, and (b) close-up of double WELs.

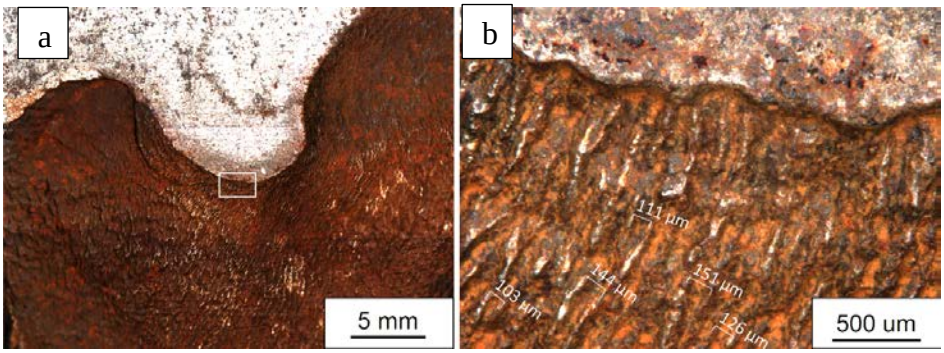

Figure 21. Images from stereomicroscopy of (a) Squat surface, and (b) detail of squat surface close to the tip of the V.

Surface topography

Mappings were done on the squat shown in Figure 21, to obtain both an overall geometry and detail mappings on smaller regions to allow for the ridges to be measured. The topographic features are presented fully in Paper 1 [30]. Additional investigation with SEM revealed crack branching in the transverse sections (e.g. Figure 22); while the longitudinal sections provide additional information about the crack geometry below the surface. Figure 23 shows undulations near the end of the crack network as compared to the detail maps.

The 3D mapping (Figure 23b) shows a highly textured surface on different scales: some beach marks, ridges, and surface roughness. It can be speculated that the ridges on the fracture surface (Figure 21b) are a result of repeated relative movement of the two crack surfaces in the same direction, while the smoother regions observed near the surface-breaking part of the crack (Figure 21a, top) are a result of rubbing of crack faces in different directions due to an additional shear displacement. This is thought to be a result of the stresses propagating the crack [14]. According to the literature, the fracture surface has both rough and smooth parts, corresponding to tension and shear crack growth, in mode I and mixed mode II/III, respectively [34].

Residues

Another squat was cross-sectioned longitudinally (parallel to the traffic direction); see Figure 24. Through optical and scanning electron microscopy, it can be seen that the cracks are filled with residues. It was found that the residues have an increased oxygen content compared with the bulk. However, elongated pearlite grains are observed around the crack faces and even within the residues (Figure 25 b and d). This suggests that the residues result in part from the crack propagation that shears bulk material that has broken off from the crack edges [35].

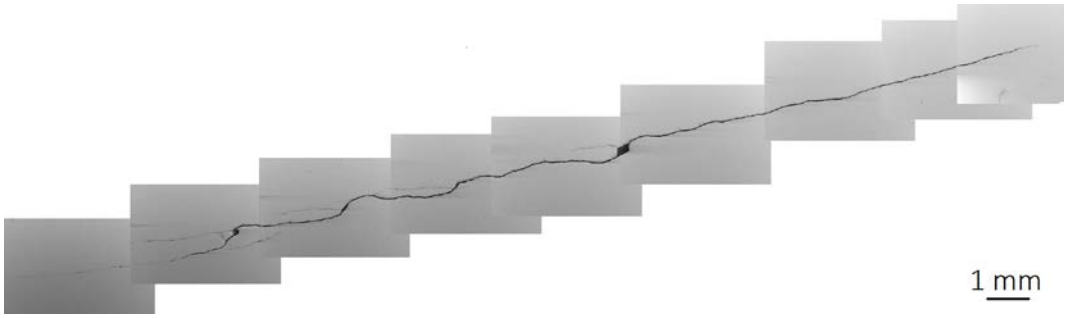

Figure 22. SEM micrographs of sections from squat in Figure 10 showing crack branching in transverse sections, not distinguishable by geometric reconstruction.

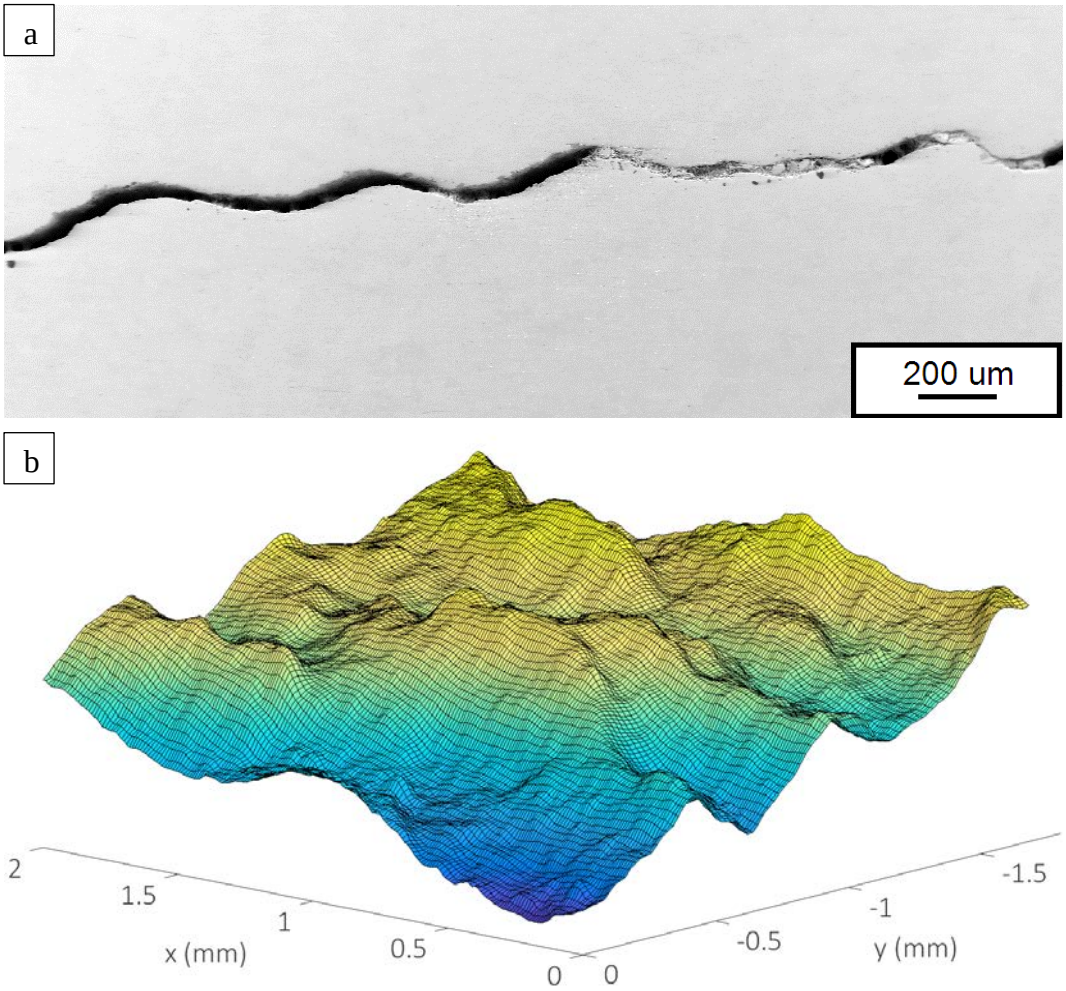

Figure 23. (a) Undulations in longitudinal section of squat network. (b) Mapping from topography showing ridges, 50-µm step size.

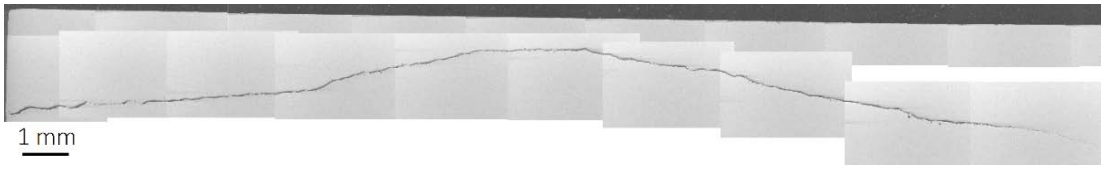

Figure 24. Longitudinal cross-section of squat.

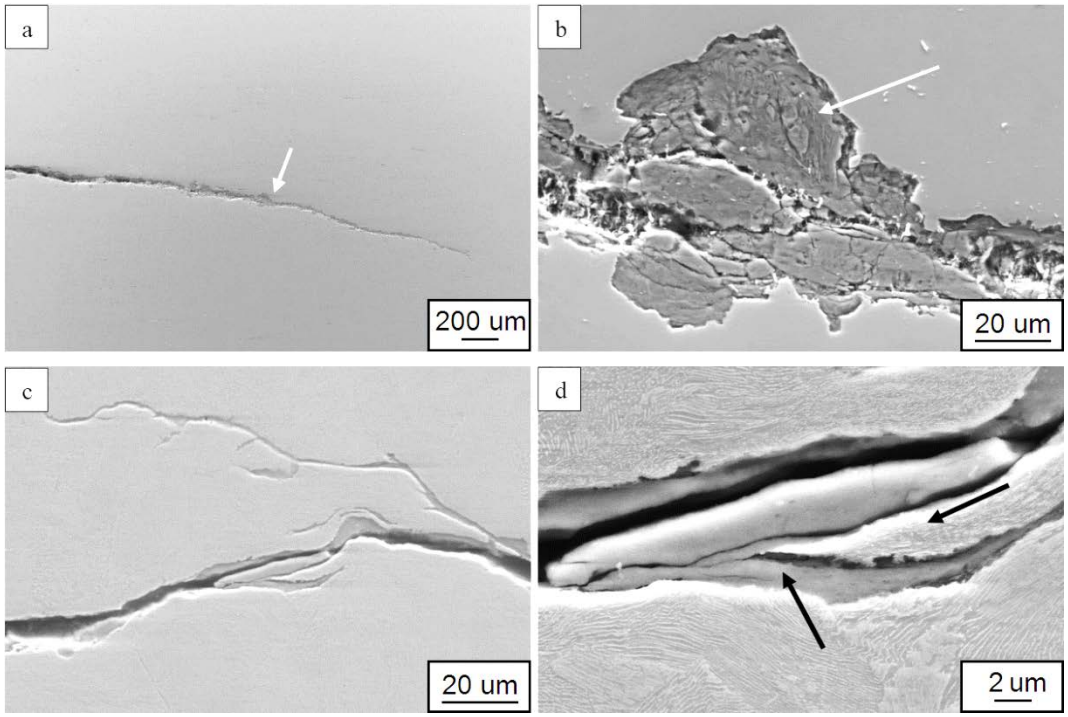

Figure 25. SEM image showing residues in cracks. a) Dark grey material near crack tip are residues, b) close-up showing deformed microstructure within the residues, c) and d) are from a transverse section of the rail.

5.2. Residual stress measurements

The residual stresses measured in the longitudinal and transverse directions are summarized in Figure 27 for the 6-mm spots on the used and new rail sections. The tests are fully documented in Paper 2. It is clear that more compressive stresses (approximately 100 MPa lower) are present in the used rails, which is expected due to plastic deformation of the surface layer of the railhead. Furthermore, comparatively high tensile stresses are present around the WEL spot on both used and new rails, and the stress value approaches zero in the center of the spots. The explanation could be linked to the thermal expansion and plastic deformation of a material volume around the spot upon heating, and volume expansion on martensite formation during subsequent cooling.

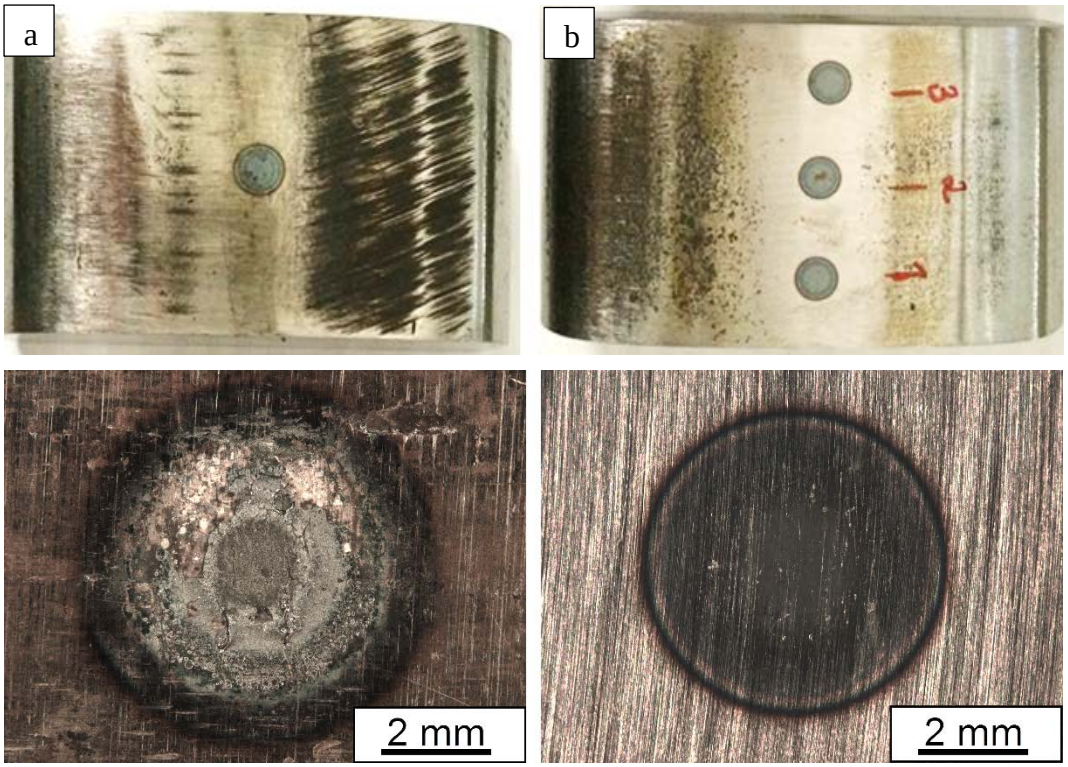

Figure 26. WEL spots on used (a) and new (c) rails.

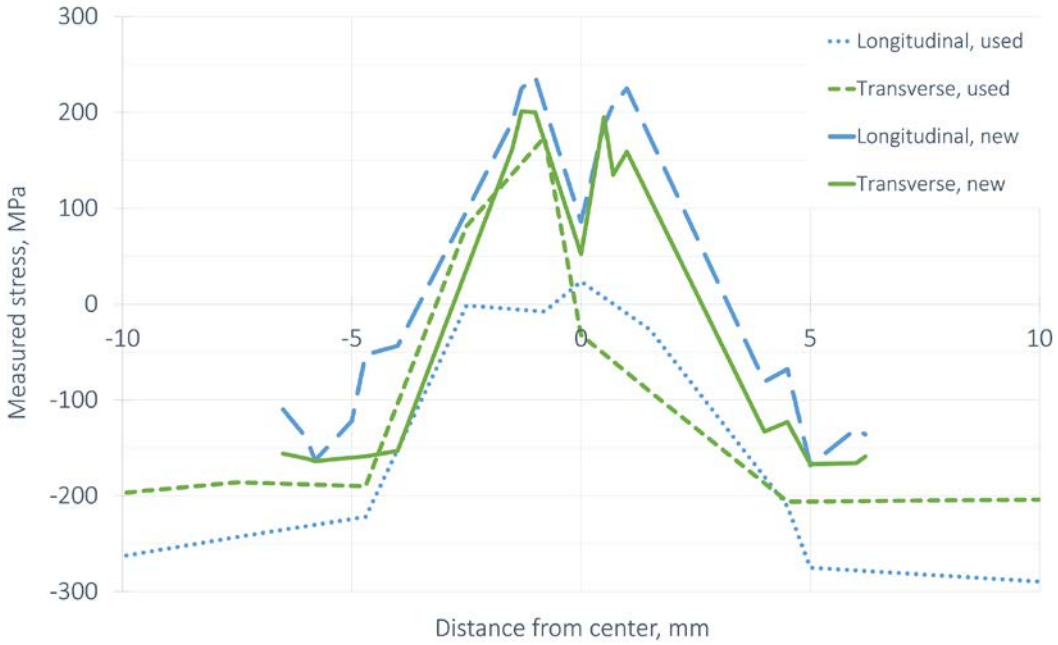

Figure 27. Surface residual stresses around 6-mm WEL spots on used and new rails.

5.3. Fatigue testing

The crack initiation and growth from different initiation types were investigated.

Effect of thermal damage

Thermal damage is an important initiation site for RCF cracking in real-life applications, and the effect was examined through controlled fatigue experiments. It was found that the presence of a small martensite spot (WEL) reduced the fatigue life of the material, Figure 28. It can be seen to acts as a stress concentration, and crack formation occurs within the spot due to the brittle nature of the martensite in comparison to the pearlite bulk material.

Effect of strain amplitude

With a constant strain rate, the effect of varied strain amplitude is reflected in peak stress differences, resulting in different fatigue lives. Increasing the peak stress for the experiments results in a reduced fatigue life (≈300 cycles at 1.5% strain amplitude, compared to ≈10 000 cycles for 0.4% strain amplitude). This is a well-known behavior and is directly linked to the fatigue theory discussed earlier in the thesis. For more details on the experimental procedure and results, please refer to Paper 2.

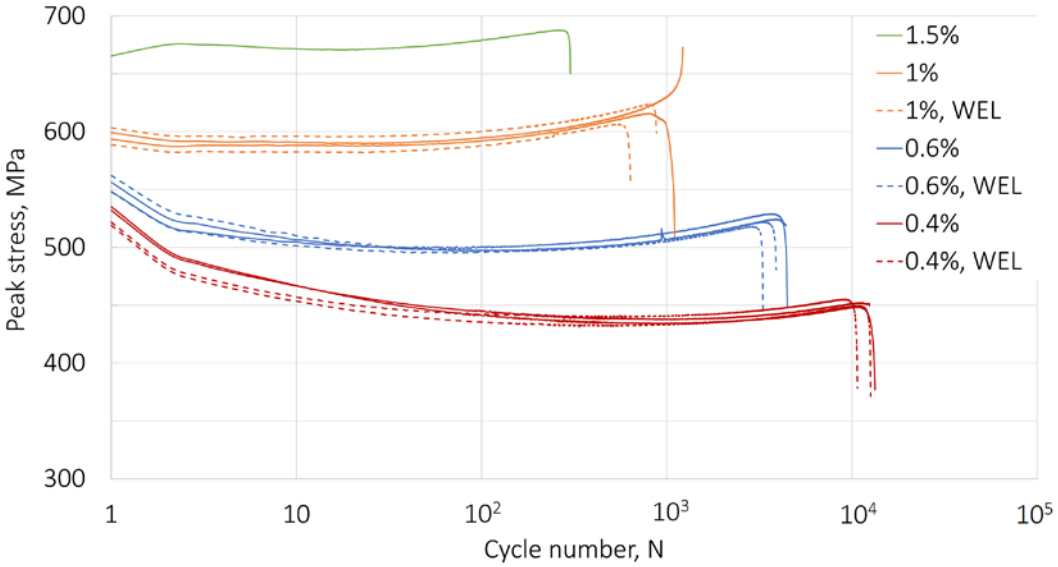

Figure 28. Peak stress evolution of LCF experiments for 0.4%, 0.6%, 1.0%, and 1.5% strain amplitude, on smooth specimens and specimens with initial thermal damage (WEL).

6. Conclusions

The aim of this PhD project can be separated into two main objectives: the first is to properly describe the 3D network of RCF defects in rails using several characterization techniques, and the second is to study crack initiation and propagation through fatigue tests. The first objective has been achieved in the work carried out so far and presented in the appended papers and in this introduction, investigating the use of X-ray radiography complemented with geometrical reconstruction, metallography, X-ray tomography, and topography measurements. It was concluded that the combination of different characterization techniques give a complete description of the squat crack network: the different methods are complementary, and observations made using one method can sometimes explain the deficiencies of other methods.

Uniaxial strain-controlled fatigue experiments investigating damage initiation from thermally affected spots in pearlitic R260 rail steel have also been presented. Characterization of the laser-induced WEL on test bars and rail sections revealed that these are similar to those found in field. Residual stress measurements around the WEL spots were generally tensile in the central parts of the WEL, decreasing to become compressive residual stresses in the bulk material. The presence of initial thermal damage, in the form of a small martensite spot (or WEL), was found to reduce fatigue life for all strain amplitudes investigated (0.4%, 0.6%, and 1%). Additionally, it was observed that failure occurs at the WEL in all cases except one, with the crack initiating in the martensite and growing outwards.

7. Future work

In order to realize the main objectives of this project, crack propagation will be studied using bi-axial fatigue tests. The goal is to continue fatigue experiments by adding torsional loading and creating bi-axial conditions similar to those present in reality. Further studies require setting up equipment for crack propagation experiments, using a conditioning chamber allowing for humidity and temperature control. The purpose of the crack propagation experiments is to examine the effects of local stress state, humidity, and temperature on fatigue crack propagation, taking into account the influence of crack-face friction.

8. References

[1] A. F. Bower and K. L. Johnson, “Plastic flow and shakedown of the rail surface in repeated wheel-rail contact,” *Wear*, vol. 144, 1991.

[2] Trafikanalys, “Rail traffic accidents 2014,” 2015.

[3] H. Schwarz, “Improving the sustainability of transport – The rail sector as a case study,” New York, 2011.

[4] R. Clark, “Rail flaw detection: overview and needs for future developments,” *NDT E Int.*, vol. 37, no. 2, pp. 111–118, 2004.

[5] Office of Rail Regulation, “Train Derailment at Hatfield: A Final Report by the Independent Investigation Board,” 2006.

[6] Railways Archive, “Accident at Hatfield on 17th October 2000.” [Online]. Available: http://www.railwaysarchive.co.uk/eventsummary.php?eventID=143. [Accessed: 07-Apr-2016].

[7] A. Hohenwarter, A. Taylor, R. Stock, and R. Pippan, “Effect of Large Shear Deformations on the Fracture Behavior of a Fully Pearlitic Steel,” vol. 42, no. June, pp. 1609–1618, 2011.

[8] A. Ekberg, B. Åkesson, and E. Kabo, “Wheel/rail rolling contact fatigue – Probe, predict, prevent,” *Wear*, vol. 314, no. 1–2, pp. 2–12, 2014.

[9] H. C. Eden, J. E. Garnham, and C. L. Davis, “Influential microstructural changes on rolling contact fatigue crack initiation in pearlitic rail steels,” *Mater. Sci. Technol.*, vol. 21, no. 6, pp. 623–629, 2005.

[10] Y. Jin Aoki, F., Ishida, M., Namura, A., “Investigation and Analysis of the Occurence of Rail Head Checks,” *Int. J. Railw.*, vol. 2, no. 2, pp. 43–49, 2009.

[11] S. L. Wong, P. E. Bold, M. W. Brown, and R. J. Allen, “A branch criterion for shallow angled rolling contact fatigue cracks in rails,” *Wear*, vol. 191, pp. 45–53, 1996.

[12] Z. Li, X. Zhao, C. Esveld, R. Dollevoet, and M. Molodova, “An investigation into the causes of squats- Correlation analysis and numerical modeling,” *Wear*, vol. 265, pp. 1349–1355, 2008.

[13] S. L. Grassie, “Squats and squat-type defects in rails: the understanding to date,” *J. Rail Rapid Transit*, vol. 226, pp. 235–242, 2011.

[14] S. L. Grassie, D. I. Fletcher, E. A. Gallardo-Hernandez, and P. Summers, “Studs: a squat-type defect in rails,” *J. Rail Rapid Transit*, vol. 226, no. 2011, pp. 243–256.

[15] W. Daniel, S. Pal, and M. Farjoo, “Rail squats: progress in understanding the Australian

experience," *J. Rail Rapid Transit*, vol. 227, no. 5, pp. 481–492, 2013.

[16] Z. Li, X. Zhao, and R. Dollevoet, "The determination of a critical size for rail top surface defects to grow into squats," *8th Internationsl Conference on Contact Mechanics and Wear of Rail/Wheel Systems*. Firenze, Italy, pp. 379–388.

[17] Z. Li, X. Zhao, R. Dollevoet, and M. Molodova, "Differential wear and plastic deformation as causes of squat at track local stiffness change with other track short defects," *Veh. Syst. Dyn.*, vol. 46, pp. 237–246.

[18] Z. Li, R. Dollevoet, M. Molodova, and X. Zhao, "Squat growth- Some observations and the validation of numerical predictions," *Wear*, vol. 271, pp. 148–157, 2011.

[19] Z. Li, "Squats on railway rails," *Wheel-rail interface handbook*, no. 13. pp. 409–436, 2009.

[20] Z. Li, X. Zhao, C. Esveld, R. Dollevoet, and M. Molodova, "The validation of some numerical predictions on squats growth," *8th International Conference on Contact Mechanics and Wear of Rail/Wheel Systems*. Firenze, Italy, pp. 369–377.

[21] J. Orlich and H. Pietrzeniuk, "Atlas zur Wärmebehandlung der Stähle, Band 4," Düsseldorf: Max-Planck-Institut für Eisenforschung: Verlag Stahleisen M.B.H., 1976, pp. 147–151.

[22] T. Eyre and A. Baxter, "The formation of white layers at rubbing surfaces," *Tribology*, pp. 256–261, 1972.

[23] H. W. Zhang, S. Ohsaki, S. Mitao, M. Ohnuma, and K. Hono, "Microstructural investigation of white etching layer on pearlite steel rail," *Mater. Sci. Eng. A*, vol. 421, pp. 191–199, 2006.

[24] J. Ahlström, "Residual stresses generated by repeated local heating events – Modelling of possible mechanisms for crack initiation," *Wear*, vol. 366–367, pp. 180–187, 2016.

[25] S. Pal, W. Daniel, A. Atrens, V. Luzin, and M. Kerr, "Role of Residual Stresses in Rail Squat Formation," 2011. [Online]. Available: http://www.ansto.gov.au/ResearchHub/Bragg/CurrentResearch/ScientificHighlights/Roleofresidualstresses/index.htm.

[26] D. A. Skoog, J. F. Holler, and S. R. Crouch, *Principles of Instrumental Analysis*, Sixth Edit. David Harris, 2007.

[27] M. E. Fitzpatrick, A. T. Fry, P. Holdway, F. A. Khadil, J. Shackleton, and L. Suominen, "Determination of Residual Stresses by X-Ray Diffraction- Issue 2," National Physical Laboratory, Teddington, Middlesex, United Kingdom, 2005.

[28] J. R. Griffiths and C. E. Richards, "Fatigue Testing," *Mater. Sci. Eng R*, vol. 11, pp. 305–315, 1973.

[29] N. E. Dowling, *Mechanical Behavior of Materials*, Fourth Edi. Pearson Education, 2013.

[30] C. Jessop, J. Ahlström, L. Hammar, S. Fæster, and H. K. Danielsen, “3D characterization of rolling contact fatigue crack networks,” *Wear*, vol. 366–367, pp. 392–400, 2016.

[31] D. Bernard, D. Gendron, J. M. Heintz, S. Bordère, and J. Etourneau, “First direct 3D visualisation of microstructural evolutions during sintering through X-ray computed microtomography,” *Acta Mater.*, vol. 53, pp. 121–128, 2005.

[32] ASTM, “Standard Test Method for Residual Stress Measurement by X-Ray Diffraction for Bearing Steels,” no. May, 2012.

[33] J. Ahlström and B. Karlsson, “Microstructural evaluation and interpretation of the mechanically and thermally affected zone under railway wheel flats,” *Wear*, vol. 232, pp. 1–14, 1999.

[34] S. Pal, W. Daniel, and M. Farjoo, “Early stages of rail squat formation and the role of a white etching layer,” *Int. J. Fatigue*, vol. 52, pp. 144–156, 2013.

[35] K. Cvetkovski, J. Ahlström, M. Norell, and C. Persson, “Analysis of wear debris in rolling contact fatigue cracks of pearlitic railway wheels,” *Wear*, vol. 314, pp. 51–56, 2014.